ACS APPLIED MATERIALS & INTERFACES

Research Article

www.acsami.org

Shell Thickness-Dependent Microwave Absorption of Core–Shell Fe_3O_4@C Composites

Yunchen Du,*[,†,‡] Wenwen Liu,[†] Rong Qiang,[†] Ying Wang,[†] Xijiang Han,[†] Jun Ma,[‡] and Ping Xu*[,†]

[†]Department of Chemistry, Harbin Institute of Technology, Harbin 150001, China

[‡]School of Municipal and Environmental Engineering, Harbin Institute of Technology, Harbin 150001, China

Supporting Information

ABSTRACT: Core–shell composites, Fe_3O_4@C, with 500 nm Fe_3O_4 microspheres as cores have been successfully prepared through in situ polymerization of phenolic resin on the Fe_3O_4 surface and subsequent high-temperature carbonization. The thickness of carbon shell, from 20 to 70 nm, can be well controlled by modulating the weight ratio of resorcinol and Fe_3O_4 microspheres. Carbothermic reduction has not been triggered at present conditions, thus the crystalline phase and magnetic property of Fe_3O_4 micropsheres can be well preserved during the carbonization process. Although carbon shells display amorphous nature, Raman spectra reveal that the presence of Fe_3O_4 micropsheres can promote their graphitization degree to a certain extent. Coating Fe_3O_4 microspheres with carbon shells will not only increase the complex permittivity but also improve characteristic impedance, leading to multiple relaxation processes in these composites, thus the microwave absorption properties of these composites are greatly enhanced. Very interestingly, a critical thickness of carbon shells leads to an unusual dielectric behavior of the core–shell structure, which endows these composites with strong reflection loss, especially in the high frequency range. By considering good chemical homogeneity and microwave absorption, we believe the as-fabricated Fe_3O_4@C composites can be promising candidates as highly effective microwave absorbers.

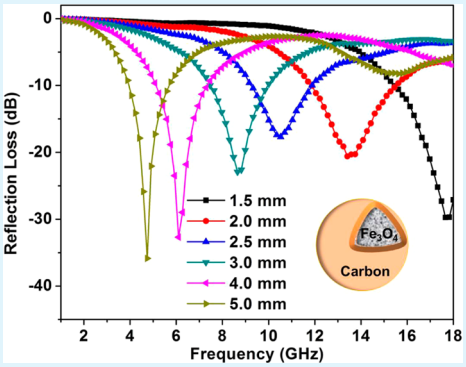

KEYWORDS: *Fe_3O_4, carbon, core–shell, composites, microwave absorption*

1. INTRODUCTION

Recent advances in the field of novel functional composites are paving the way for exciting applications in modern science and technology, because composite materials not only inherit the properties from their individuals, but also provide the possibility for enhanced functionality and multifunctional properties owing to the interaction between individual parents.[1−5] During the past decades, there has been a tremendous increase in constructing composites based on iron oxides particles because of their compatible magnetic and electrochemical properties, which endowed these composites with potential applications in many fields, such as Li-ion batteries, microwave absorption, catalysis, absorption and separation, biosensors, etc.[6−12] Among those composites, Fe_3O_4/C composites have received much attention as a result of tunable properties and highly chemical stability of carbon materials, as well as significant synergetic or complementary behavior between Fe_3O_4 and carbon. Up to now, various carbon materials, for example, carbon nanotubes, carbon nanofibers, mesoporous carbon, graphene, have been extensively utilized as main components of Fe_3O_4/C composites.[13−17]Although expected improvement in property can be achieved by these composites, it is important to mention that Fe_3O_4 particles are usually distributed in carbon matrix in a random way, and the poor chemical homogeneity will not be favorable for their practical applications.[18,19]

More recently, many scientists have shown their interests in constructing core–shell structures as an effective route to improve the chemical homogeneity and enhance the functionality of Fe_3O_4/C composites.[20−28] For example, Xuan et al. designed a simple method for Fe_3O_4@C composites under hydrothermal conditions by using glucose as both the reducing agent and carbon precursor, where the amount of glucose had a great impact on the morphology of the final products;[20] Li et al. transformed Fe_2O_3@PAA nanoparticles into core–shell Fe_3O_4@C chains and rings by high-temperature carbothermic reduction, and the unique microstructure endowed them with high reversible capacity and good cycling stability as electrode materials;[21] An et al. chose ferrocene as the single regent to produce core–shell Fe_3O_4@C microspheres under hydrothermal conditions, which could be used as highly active SERS substrate after decorating with Ag nanoparticles on their surface;[22] Zhang et al. and You et al. employed Stöber method and microwave hydrothermal method, respectively, to manipulate the synthesis of core–shell Fe_3O_4@C composites with tunable carbon shell thickness.[23,24]

As mentioned above, Fe_3O_4/C composites have been taken as one of the popular topics in microwave absorbers because

Received: May 12, 2014
Accepted: July 22, 2014
Published: July 22, 2014

they combine magnetic loss ability and dielectric loss ability effectively, which is quite beneficial to improve microwave absorption.[29−33] In comparison with conventional Fe_3O_4/C composites, core−shell Fe_3O_4@C composites show superior chemical homogeneity and structural advantages, thus it will be promising and meaningful to develop the microwave absorption of core−shell Fe_3O_4@C composites,[34] especially to investigate the effect of the carbon shell thickness on the electromagnetic properties systematically. Unfortunately, there are very few correlative literatures accessible.

In this article, we demonstrate the synthesis of core−shell Fe_3O_4@C composites and investigate their microwave absorption. The thickness of carbon shell can be well controlled in the range of ∼20−70 nm by modulating the amount of resorcinol and formaldehyde. It is realized that introduction of carbon shell can effectively increase dielectric loss properties and improve matching characteristic impedance of the composites, resulting in enhanced microwave absorption performances. More interestingly, microwave absorption properties and dielectric behaviors of the Fe_3O_4@C composites can be easily tuned by the shell thickness. Especially when the thickness of carbon shells reaches a critical point, there will be an unusual dielectric behavior arising from the core−shell structure, which endows these composites with strong reflection loss in the corresponding frequency range.

2. EXPERIMENTAL SECTION

2.1. Synthesis of Fe_3O_4 Microspheres. Fe_3O_4 microspheres were prepared by solvothermal method similar to a previous literature.[35] Briefly, 5.40 g of $FeCl_3{\cdot}6H_2O$ and 10.0 g of sodium acetate were dissolved in 140 and 60 mL of ethylene glycol, respectively. And then, two solutions were mixed and stirred for 0.5 h. The obtained homogeneous yellow solution was transferred into a Teflon-lined stainless-steel autoclave and sealed to heat at 200 °C for 24 h. The obtained black magnetite particles were washed with distilled water and absolute ethanol to remove any residues, and then dried at 50 °C.

2.2. Synthesis of Core−Shell Fe_3O_4@C Composites. The Fe_3O_4@C core/shell microspheres were prepared by in situ polymerization and high-temperature carbonization. In a typical recipe, 1.0 g of Fe_3O_4 microspheres were dispersed in a stock solution, which contains 80 mL of water, 32 mL of absolute ethanol, and 0.4 mL of ammonia, and the mixed solution was treated by ultrasonication for 1 h to produce a uniform suspension. Then, the required amount of resorcinol was added into the solution. The mixture was mechanically stirred at room temperature for 30 min before adding formaldehyde solution (38 wt %) to start the polymerization for another 24 h. The obtained Fe_3O_4@phenolic resin composites were collected by magnetic separation and redispersed in distilled water under ultrasonication. This process was repeated at least three times until the water phase after sample collection became colorless, and then the composites were dried in a vacuum drier at 50 °C. Finally, the Fe_3O_4@phenolic resin composites were carbonized in a horizontally tubular furnace under N_2 atmosphere at 350 °C for 2 h and 650 °C for 2 h, where the heating rate was controlled at 1 °C/min. Through the experiments, the molar ratio of resorcinol to formaldehyde was fixed at 1:2. The product samples were denoted as S1, S2, S3 S4, S5, where the amounts of resorcinol were 0.1, 0.2, 0.3, 0.4, and 0.6 g, respectively.

2.3. Characterization. Powder X-ray diffraction (XRD) data were recorded on an XRD-6000 X-ray diffractometer (Shimadzu) with a Cu Kα radiation source (40.0 kV, 30.0 mA). The thermogravimetric analysis was carried out on a SDT Q600 TGA (TA Instruments) in the temperature range of room temperature to 800 °C ata heating rate of 10 °C/min. Scanning electron microscope (SEM) images were obtained on anQuanta 200S (FEI), and the samples were mounted on aluminum studs by using adhesive graphite tape and sputtercoated with gold before analysis. Transmission electron microscope (TEM) images were obtained on a Tecnai G^2 F30 operating at an accelerating voltage of 200 kV. Raman spectra were performed on a confocal Raman spectroscopic system (Renishaw, In Via) using a 633 nm laser. An HP-8722E vector network analyzer was applied to determine the relative permeability and permittivity in the frequency range of 1−18 GHz for the calculation of reflection loss. A sample containing 50 wt % of obtained composites was pressed into a ring with an outer diameter of 7 mm, an inner diameter of 3 mm, and a thickness of 2 mm for microwave measurement in which paraffin wax was used as the binder.

3. RESULTS AND DISCUSSION

During the high-temperature carbonization process, phenolic resin can be converted into carbon species through pyrolysis.[36] It is well-known that there are possible interactions between carbon species and iron oxides under high-temperature conditions, where carbon species can induce carbothermic reduction to produce metal Fe, while iron oxides or metal Fe may promote the graphitization degree of carbon materials, even to generate crystalline graphite.[37] Therefore, it is primarily important to determine the crystalline phases of various composites. As shown in Figure 1, all composites exhibit

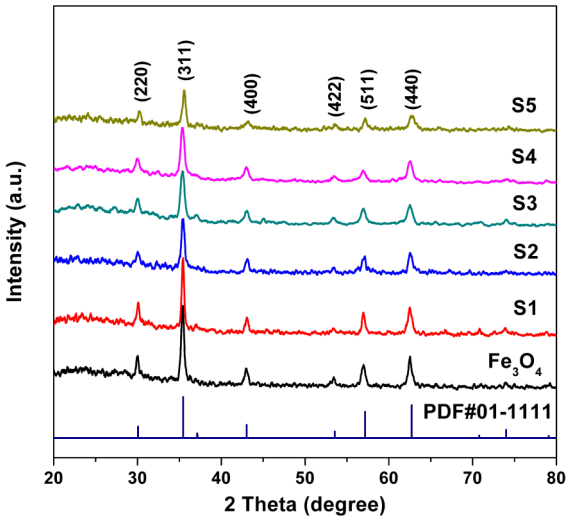

Figure 1. XRD patterns of Fe_3O_4 microspheres and different core−shell Fe_3O_4@C composites.

XRD peaks at ∼30.0°, 35.4°, 43.0°, 53.4°, 57.0°, 62.5°, which can be typically indexed to the spinel phase of Fe_3O_4 (JCPDS 01-1111),[38] indicating the Fe_3O_4 phase can be well preserved during the carbonization process. Meanwhile, no evident differences can be found between pristine Fe_3O_4 microspheres and these composites. Particularly, the absence of characteristic peaks assigned to crystalline graphite in these composites implies the amorphous nature of carbon components in these composites. These results suggest that chemical interactions between carbon species and iron oxides do not occur under current conditions (650 °C, N_2 atmosphere). It is important to point out that when the carbonization temperature increases to 700 °C, the carbothermic reduction will be ignited drastically, and one can obtain single phase of metal Fe without any residuals of Fe_3O_4 phase (Supporting Information Figure S1).

Figure 2 shows the morphology evolution of Fe_3O_4@C composites with different carbon content. Through the typical process, obtained Fe_3O_4 microspheres are fully composed of spherical particles with an average diameter of about 500 nm (Figure 2a), and these microspheres are essentially assembled by nanoparticles that are less than 30 nm in size (Supporting

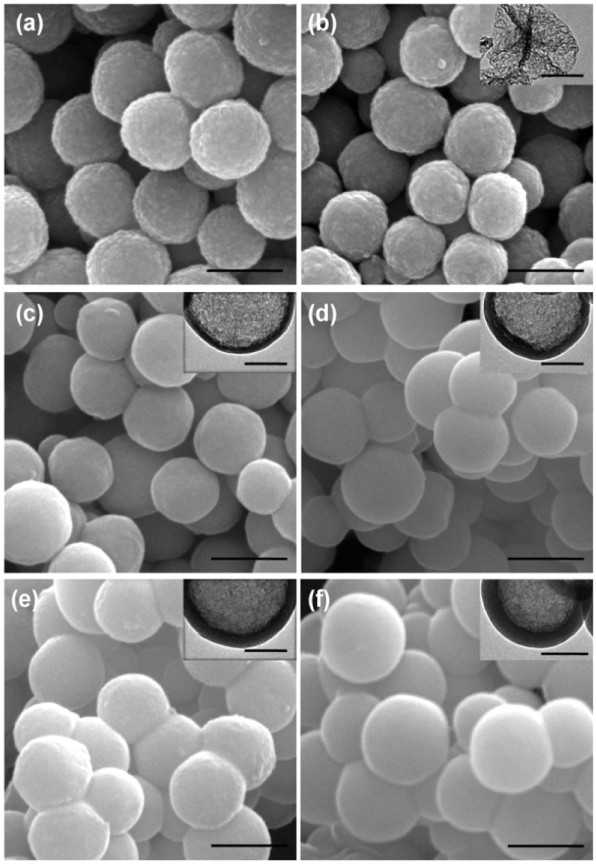

Figure 2. SEM images of Fe_3O_4 microspheres (a) and different core–shell Fe_3O_4@C composites: S1 (b), S2 (c), S3 (d), and S4 (e), and S5 (f). Inset in each SEM image is the TEM image showing the thickness of the carbon shell after Fe_3O_4 is removed by acid treatment. Scale bars in SEM and TEM images are 500 and 200 nm, respectively.

Information Figure S2). Using the as-prepared Fe_3O_4 microspheres as cores, carbon coating can be achieved on these microspheres through in situ polymerization of phenolic resin following by a carbonization process, producing composites with core–shell structures. It should be mentioned that although there is carbon coating on the surface, the particle size of S1 is a little smaller than that of as-prepared Fe_3O_4 microspheres, resulting from a shrinkage of Fe_3O_4 microspheres during the high-temperature carbonization process.[39] The sizes of the core–shell composites display monotonic increase with more resorcinol and formaldehyde applied in the experiments. When the amount of resorcinol reaches 0.3 g (S3, Figure 2d), adherence between adjacent microspheres appears in the composites, but further aggregation is still avoided because noncoating phenolic resin has been eliminated effectively by our magnetic separation process. In order to better understand the thickness of carbon shell in these composites, we removed the Fe_3O_4 cores by strong acid treatment. As shown in the TEM images inset in Figure 2, one can see that the thicknesses of carbon shells for S2, S3, S4, and S5 are about 20, 30, 42, and 66 nm, respectively, while the carbon shell of S1 collapses after removing the Fe_3O_4 cores due to its low carbon content. Our results indicate that with proper control of the experimental conditions and relative ratios of resorcinol to Fe_3O_4 microspheres, carbon shells can be successfully fabricated on the cores and more importantly, the shell thickness can be modulated at the nanoscale. Low-magnification TEM images and statistical data (Supporting Information Figure S3) demonstrate that the distributions of carbon-shell thickness in S2, S3, and S4 are quite narrow, while it becomes a little wide in S5. Besides, we also observe some sporadic carbon spheres in S5 (Supporting Information Figure S4), which implies that this may be the critical point for the formation of core–shell Fe_3O_4@C structures. If more resorcinol is applied, we will get Fe_3O_4@C composites with more pure carbon spheres and nonuniform carbon shells, but not isolated core–shell structures.

From the thermogravimetric (TG) curves in Figure 3, one can see two weight losses due to the removal of adsorbed water

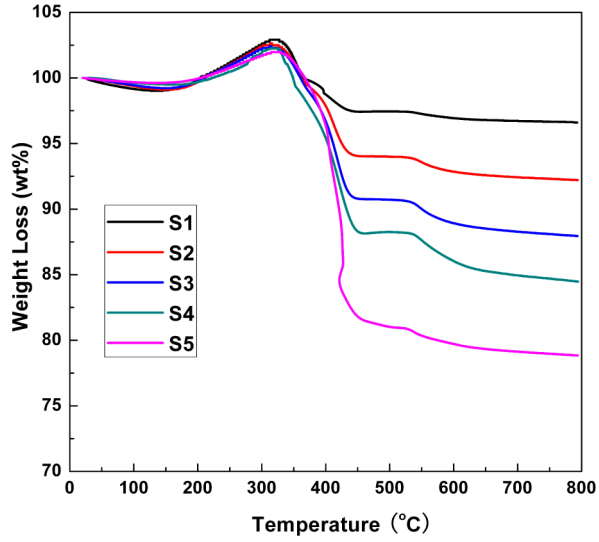

Figure 3. TG curves of different core–shell Fe_3O_4@C composites, where the actual carbon contents of S1, S2, S3, S4, and S5 are calculated to be 5.64, 9.97, 14.20, 17.84, and 23.41 wt %, respectively.

(about 150 °C) and combustion of carbon (starting at about 320 °C), and one weak weight increase region (transformation of Fe_3O_4 to Fe_2O_3) in the temperature range of ~150–320 °C.[40] As carbon components can be completely burned in air, the final product will be only Fe_2O_3. Therefore, the amount of carbon in these composites can be calculated by[35]

$$\text{wt \% } R = (1 - \text{wt \% carbon} - \text{wt \% water})\frac{1.5M(Fe_2O_3)}{M(Fe_3O_4)} \quad (1)$$

where wt % R is the remaining weight percentage after combustion, and M indicates the molecular weight of the compound. As deduced from eq 1, the weight percentages of carbon in these composites, S1, S2, S3 S4, and S5, are 5.64, 9.97, 14.20, 17.84, and 23.41 wt %, respectively. This indicates that the actual carbon content in the composites is somehow lower than that as designed. It can be rationalized by the fact that (1) water-soluble oligomers can inevitably be produced during the polymerization reaction, which can then be removed during the washing procedures; (2) phenolic resin without coating on the Fe_3O_4 microspheres can also be formed, which cannot be collected using the magnetic separation technique. Therefore, we normally get less carbon in the Fe_3O_4@C composites.

Figure 4 shows the hysteresis loops of Fe_3O_4 microspheres and Fe_3O_4@C core–shell composites measured at 300 K. The as-prepared Fe_3O_4 microspheres, with a saturation magnet-

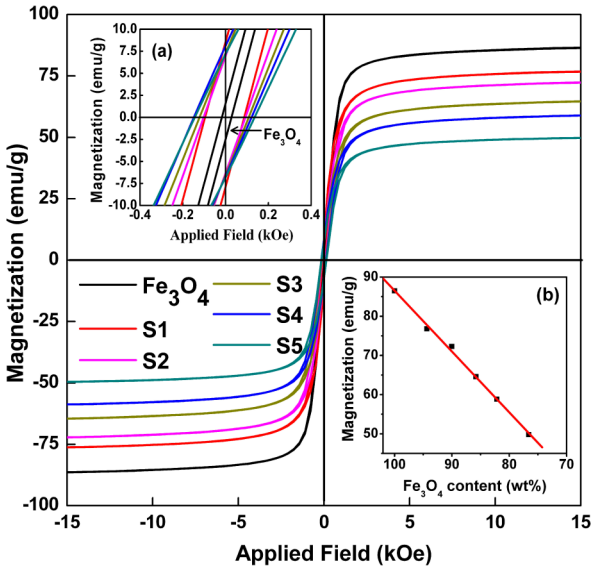

Figure 4. Magnetic properties of Fe_3O_4 microspheres and different core−shell Fe_3O_4@C composites. Insets a and b are the local enlargement and the relationship between saturation magnetization and Fe_3O_4 content in the composites, respectively.

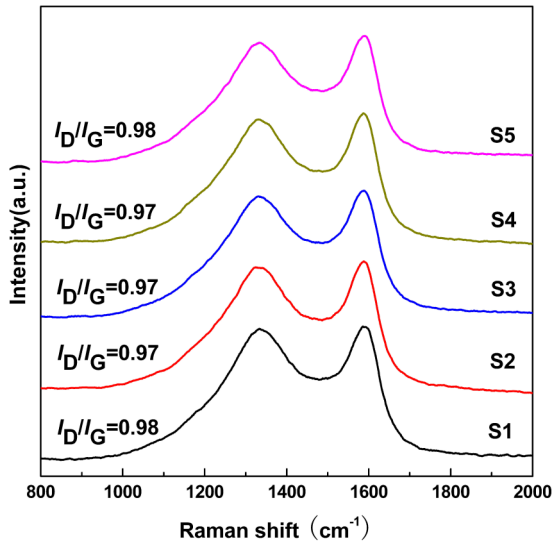

Figure 5. Raman spectra of carbon shells from different core−shell Fe_3O_4@C composites.

ization (M_s) of 86.3 emu/g, display a quasi superparamagnetic characteristic, with rather small remanent magnetization (<2 emu/g) andcoercivity (ca. 20 Oe), suggesting that the Fe_3O_4 microspheres are actually formed by an assembly of small nanoparticles, which is highly consistent with the result of TEM (Supporting Information Figure S2).[38,41] It can be seen that the remanent magnetization and coercivity increases to about 8 emu/g and 140 Oe (Figure 4, inset a), respectively, after the Fe_3O_4 microspheres are coated by carbon shell. We believe it can be attributed to the size growth of nanoparticles in Fe_3O_4 microspheres during the high-temperature carbonization process,[42] although the slight change in particles sizes has not been detected by XRD. M_s values of S1, S2, S3, S4, and S5 are 76.8, 72.3, 64.6, 58.9, and 49.8 emu/g, respectively; namely, the less carbon content, the stronger *Ms* values of the composites. From the relationship between M_s value and Fe_3O_4 microspheres content (Figure 4, inset b), a quasi linear decrease in M_s can be found with decreasing the Fe_3O_4 microspheres content in composites, which can be easily understood by the fact that the carbon shell will not affect the magnetic nature of the composites, but just reduce the content of Fe_3O_4 microspheres. These results again verify that Fe_3O_4 can be well maintained in the preparation process.

Generally, graphitization degree of carbon component will have a great impact on the electromagnetic parameters and microwave absorption of carbon-containing absorbers.[43,44] As shown by the Raman spectra (Figure 5), all Fe_3O_4@C composites display two distinguishable peaks in the range of 1000−2000 cm^{-1}, one broad peak centered at about 1350 cm^{-1} (*D* band), and one other relatively sharp peak at about 1590 cm^{-1} (*G* band). It is very interesting that the values of the intensity ratios of these two bands, I_D/I_G, are almost identical in all Fe_3O_4@C composites, which is a hint that carbon components in these composites have nearly same graphitization degree. However, pristine carbon materials, which are prepared under the same conditions as Fe_3O_4@C composites except the presence of Fe_3O_4 microspheres, give an I_D/I_G value of 0.92 (Supporting Information Figure S5). According to previous literatures,[45,46] *D* band is a breathing mode of A_{1g} symmetry involving phonons near the *K* zone boundary, which is forbidden in perfect graphite and becomes active in the presence of disorder or finite-size crystals of graphite (nanographite crystals); *G* band corresponds to the E_{2g} mode due to stretching vibrations of sp^2 bond, which can be produced by all sp^2 sites and not only by graphitic carbon. Ferrari and Robertson once interpreted Raman spectra of amorphous carbon in detail and proposed a three-stage model based on the variation of the value of I_D/I_G, where the increased values of I_D/I_G in amorphous carbon could be the transitional stage from amorphous carbon to nanocrystalline graphite.[47] That is to say, the presence of Fe_3O_4 has stimulated the formation of nanocrystalline graphite in these composites, resulting in a little higher graphitization degree of carbon component than that of pristine carbon. However, it has been reported that these nanocrystalline graphite cannot be detected even by high-resolution TEM techniques.[48]

Microwave absorption properties of a absorber are highly associated with its complex permittivity and complex permeability, where the real parts of complex permittivity (ε') and complex permeability (μ') represent the storage capability of electric and magnetic energy, and imaginary parts (ε'' and μ'') stand for the loss capability of electric and magnetic energy.[49,50] Figure 6 shows the complex permittivity of all Fe_3O_4@C composites in the frequency range 1−18 GHz. ε' and ε'' of bare Fe_3O_4 microspheres are almost constant throughout the whole frequency range except for a very weak resonance behavior at about 13.0 GHz. ε'' values are very close to zero, indicating very poor dielectric loss of Fe_3O_4 microspheres. With the increase of carbon content, both ε' and ε'' are obviously enhanced and become more and more dependent on the frequency. This enhancement can be attributed to higher electrical conductivity of carbon shell than that of Fe_3O_4 microspheres, which is favorable for high complex permittivity according to the free electron theory.[51] It has to point out that pristine carbon materials, e.g. graphene, mesoporous carbon, carbon nanocoils, carbon nanotubes, carbon fibers, generally display a frequency dispersion behavior in the range of 1−18 GHz, that is, their complex permittivity will gradually decrease with the increasing frequency.[43,44,52−55]

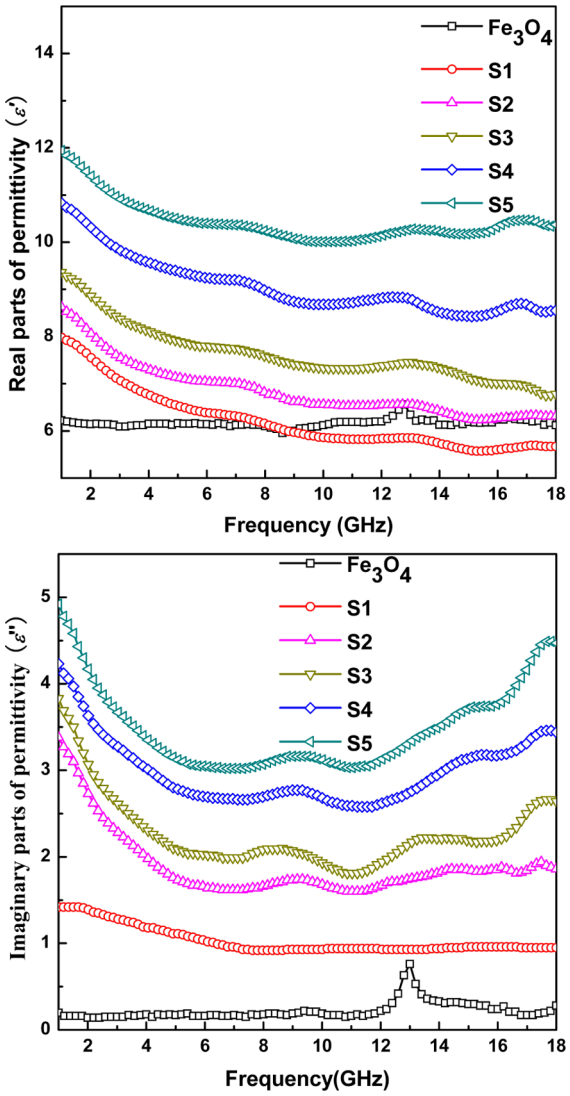

Figure 6. Real parts (ε') and imaginary parts (ε'') of the complex permittivity of Fe_3O_4 microspheres and different core–shell Fe_3O_4@C composites in the frequency range of 1–18 GHz.

This frequency dispersion behavior will still exist in most composites of carbon materials with different magnetic components. In our case, all Fe_3O_4@C composites also have common frequency dispersion behavior in ε' values, except that the variation of ε' values for S5 is negligible in the range of 8–18 GHz. However, it is very interesting that ε'' values in Fe_3O_4@C composites show a distinguishable frequency-dependence behavior. For example, ε'' values of S1 decrease from 1.42 at 1 GHz to 0.96 at 7.6 GHz and keep constant in the rest of frequency range; ε'' values of S2 decrease from 3.38 at 1 GHz to 1.62 at 7.30 GHz and then present a small fluctuation with a maximum of 1.94 at 17.5 GHz; when the carbon content is further increased, ε'' values increase gradually in the range of 11–18 GHz and the curves of ε'' value vs frequency become obviously concave, implying that these composites may have better dielectric loss abilities in the corresponding frequency range. Considering that the unique dielectric behavior is rarely observed in common composites, it is reliable to attribute this phenomenon to the carbon-based core–shell structure. Similar results have occasionally appeared in some previous reports about core–shell composites of carbon and magnetic metals, but without being paid special attention.[56−59] In our opinion, this phenomenon may be explained from the following aspects. On one hand, the amorphous nature of carbon shell will result in many defects on its surface, which can be the polarization centers under the microwave irradiation.[60] On the other hand, interfacial polarization and associated relaxation at the interfaces will happen between the core and the shell.[34] Through the cooperation of different polarization models and relaxation process, a large amount of charges can accumulate at the interfaces, especially when the carbon shell possesses enough thickness, there will be enough charges that can reverse the conventional dielectric behavior of carbon component under the assistance of the applied electromagnetic field. In one word, all of these results indicate that carbon shell plays a dominant role in determining the dielectric loss properties of these core–shell composites.

Figure 7 shows the μ' and μ'' of all Fe_3O_4@C composites in the frequency range 1–18 GHz. Bare Fe_3O_4 microspheres

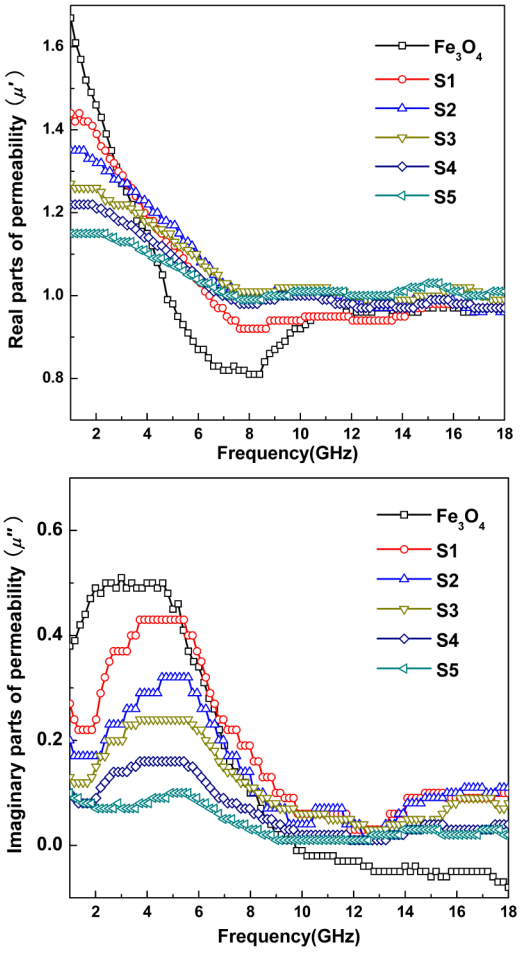

Figure 7. Real parts (μ') and imaginary parts (μ'') of the complex permeability of Fe_3O_4 microspheres and different core–shell Fe_3O_4@C composites in the frequency range of 1–18 GHz.

exhibit an abruptly decreased μ' values from 1.74 at 1 GHz to 0.82 at 7.6 GHz, and then gradually increases to 0.97 at 18 GHz; while the μ'' values increase from 0.38 at 1 GHz to a maximum of about 0.5 at 3 GHz, and then sharply decrease to 0 at 10 GHz and keep negative in the range of 10–18 GHz, implying that there is a normal resonance phenomenon between μ' and μ''. It can be seen that complex permeabilities

dx.doi.org/10.1021/am502910d | ACS Appl. Mater. Interfaces 2014, 6, 12997−13006

of Fe_3O_4@C composites display the same trend as that of Fe_3O_4 microspheres, but there are intersecting points in the curves of both real parts and imaginary parts between Fe_3O_4 microspheres and Fe_3O_4@C composites. For example, increasing the thickness of carbon shell (carbon content) endows Fe_3O_4@C composites with higher μ' values at relatively high frequencies, particularly in the range of 4−10 GHz, whereas inverse changes are distinguished over 1−4 GHz; the intersecting point becomes 10 GHz in μ'' curves, beyond which Fe_3O_4 microspheres give smaller μ'' values. As can be learned, Fe_3O_4@C composites inherit the normal resonance phenomenon and magnetic loss ability of Fe_3O_4 microspheres, although they are gradually attenuated with increasing thickness of carbon shell. It can be expected that the inherited magnetic loss from Fe_3O_4 microspheres together with the derived dielectric loss from carbon shell will bring effective enhancement in the reflection loss of incident electromagnetic waves.

On the basis of the measured data of the complex permittivity and complex permeability (Figures 6 and 7), the reflection loss properties (R(dB)) of Fe_3O_4@C composites can be deduced from the transmission line theory,

$$R\ (\mathrm{dB}) = 20 \log \left| \frac{Z_{in} - 1}{Z_{in} + 1} \right| \tag{2}$$

Z_{in} refers to the normalized input impedance of a metal-backed microwave absorbing layer and is given by[35,50]

$$Z_{in} = \sqrt{\frac{\mu_r}{\varepsilon_r}} \tanh\left[j\left(\frac{2\pi}{c}\right) fd\sqrt{\mu_r \varepsilon_r} \right] \tag{3}$$

where ε_r ($\varepsilon_r = \varepsilon' - j\varepsilon''$) and μ_r ($\mu_r = \mu' - j\mu''$) are the complex permittivity and permeability respectively, of the composite medium, c is the velocity of electromagnetic waves in free space, f is the frequency of microwave, and d is the thickness of an absorber. Figure 8 shows the calculated reflection loss of Fe_3O_4@C composites with a thickness of 2 mm in the frequency range of 1−18 GHz, where the reflection loss properties are sensitive to the thickness of carbon shell. Bare Fe_3O_4 microspheres exhibit poor reflection loss characteristics, typically less than −5 dB in the whole frequency range. Although the carbon content of S1 is too limited (5.64 wt %) to form complete shell structure, it still stimulates the enhancement of microwave absorption, where the maximum reflection loss can reach −9.6 dB at 16.8 GHz. As observed, the reflection loss properties toward incident electromagnetic waves of Fe_3O_4@C composites are enhanced substantially with further increasing the thickness of carbon shell and the frequency relating to the maximum reflection loss are also dependent on the thickness of carbon shell in these composites. The maximum reflection losses of S2, S3, S4, and S5 are −18.8, −18.1, −20.6, and −20.0 dB at 15.8, 14.4, 13.4, and 12.1 GHz, respectively, and the bandwidths exceeding −10 dB (90% absorption) for these composites are 13.8−18.0, 12.9−17.8, 11.8−15.6, and 10.9−13.6 GHz.

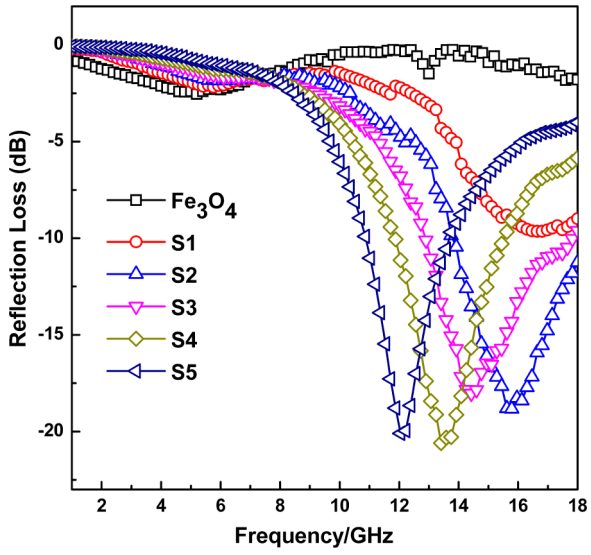

Figure 8. Microwave reflection losses (absorber thickness = 2 mm) of Fe_3O_4 microspheres and different core−shell Fe_3O_4@C composites in the frequency range of 1−18 GHz.

It is widely accepted that microwave absorption properties may be ascribed to several factors, such as magnetic loss, dielectric loss, characteristic impedance, interface relaxation, etc.[61] The magnetic loss of magnetic materials mainly originates from hysteresis, domain wall resonance, natural ferromagnetic resonance, and eddy current effect.[62] The hysteresis loss is negligible in the weak field, and the domain wall resonance loss usually occurs at much lower frequency (MHz).[63] Therefore, the natural ferromagnetic resonance and the eddy current effect are two important parameters that should be considered in this study. Bare Fe_3O_4 microspheres exhibit a natural ferromagnetic resonance in the range of 1−10 GHz, while it is further attenuated with increasing the thickness of carbon shell (Figure 7). The eddy current loss can be evaluated by eq 4,[64,65]

$$\mu'' = 2\pi\mu_0(\mu')^2\sigma \cdot d^2 f/3 \tag{4}$$

where σ (S·m^{-1}) is the electrical conductivity and μ_0 (H·m^{-1}) is the permeability in vacuum. If the reflection loss results from the eddy current effect, the values of C_0 ($C_0 = \mu''(\mu')^{-2}f^{-1}$) are constant when the frequency is changing. As shown in Supporting Information Figure S6, the values of C_0 for bare Fe_3O_4 microspheres and core−shell Fe_3O_4 composites are almost constant in the range of 10−18 GHz, confirming the presence of the eddy current loss. However, bare Fe_3O_4 microspheres, with both strong natural ferromagnetic resonance and eddy current effect, only show poor microwave absorption (Figure 8), indicating that the contribution of magnetic loss to microwave absorption is rather limited.

Figure 9 shows dielectric dissipation factors ($\tan \delta_e = \varepsilon''/\varepsilon'$) of Fe_3O_4 microspheres and Fe_3O_4@C core−shell composites. Bare Fe_3O_4 microspheres show quite low dielectric dissipation factor in the whole frequency range due to its small ε'' values (Figure 6), and a small peak at about 13.0 GHz arising from the resonance behavior of complex permittivity can also be observed. With the introduction of carbon species, Fe_3O_4@C composites show improved dielectric dissipation factors, especially when complete carbon shells are formed on the surface of Fe_3O_4 microspheres, the dielectric dissipation factors increase gradually with the thickness of carbon shell until the thickness of carbon shell reaches about 40 nm (S4). Further increasing the thickness of carbon shell cannot enhance the dielectric dissipation factor obviously. Very importantly, the results of microwave absorption are highly consistent with the variation of dielectric dissipation factors, which means that dielectric loss plays an important role in microwave absorption of Fe_3O_4@C composites. Although dielectric loss contributes to the microwave absorption positively, it has to point out that the

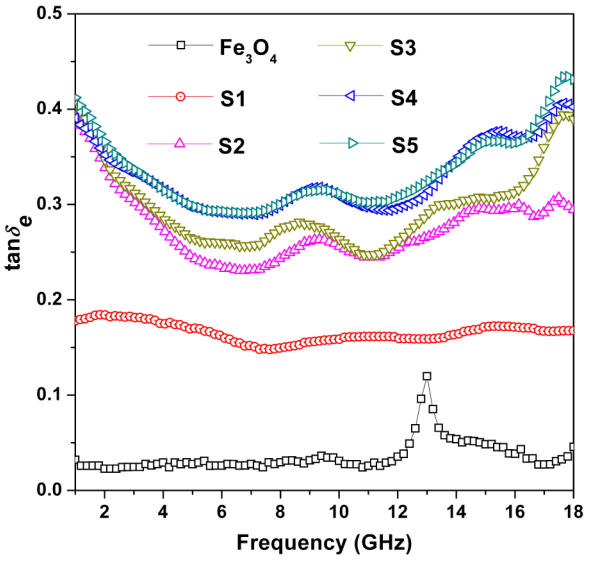

Figure 9. Dielectric dissipation factors ($\tan \delta_e$) of Fe_3O_4 microspheres and different core–shell Fe_3O_4@C composites in the frequency range of 1–18 GHz.

ε'' values and dielectric dissipation factors of these composites are not outstanding, and even inferior as compared with some existing literatures.[18,32,53] There is another important parameter relating to the considerable reflection loss from the Fe_3O_4@C composites, the concept of matched characteristic impedance, which is determined by the relationship between complex permittivity and complex permeability.[66] In other words, when the microwave absorbers have some dielectric and magnetic loss abilities, the key point for their microwave absorption will be the relationship between complex permittivity and complex permeability. Specifically, if complex permittivity is much higher than the complex permeability, most of incident microwave will be reflected off at the surface due to high surface resistance; on the contrary, incident microwave will go through the absorbers without any dissipation.[43] For example, Fe_3O_4 microspheres herein exhibit some magnetic loss abilities, but their imaginary parts of complex permittivity are too low to produce acceptable reflection loss characteristics (Figure 7). As the thickness of carbon shell increases, the complex permittivity of composites is enhanced gradually, so that the characteristic impedance is improved effectively. Considering that the values of complex permeability from Fe_3O_4 microspheres are not high, the complex permittivity from carbon component should be controlled in a rational range. Otherwise, the characteristic impedance will not be well matched, and only poor microwave absorption can be produced. Therefore, the improved characteristic impedance should also be responsible for the enhancement of microwave absorption.

Moreover, some studies stated that Debye dipolar relaxations were also favorable for the enhancement of microwave absorption.[50−52] According to Debye theory, the complex permittivity (ε_r) can be written as,[51]

$$\varepsilon_r = \varepsilon' + i\varepsilon'' = \varepsilon_\infty + \frac{\varepsilon_s - \varepsilon_\infty}{1 + i\omega\tau_0} \quad (5)$$

where τ_0, $\varepsilon_{s,\text{ and}}$ ε_∞ are the relaxation time, the static dielectric constant, and the dielectric constant at infinite frequency, respectively. From eq 5, it can be deduced that

$$\varepsilon' = \varepsilon_\infty + \frac{\varepsilon_s - \varepsilon_\infty}{1 + (\omega\tau_0)^2} \quad (6)$$

$$\varepsilon'' = \frac{\omega\tau_0(\varepsilon_s - \varepsilon_\infty)}{1 + (\omega\tau_0)^2} \quad (7)$$

It can be further deduced from eq 6 and 7 that

$$(\varepsilon' - \varepsilon_\infty)^2 + (\varepsilon'')^2 = (\varepsilon_s - \varepsilon_\infty)^2 \quad (8)$$

Therefore, the plot of ε'' versus ε' would be a single semicircle, generally denoted as the Cole–Cole semicircle. Each semicircle corresponds to a Debye dipolar relaxation. Figure 10 shows

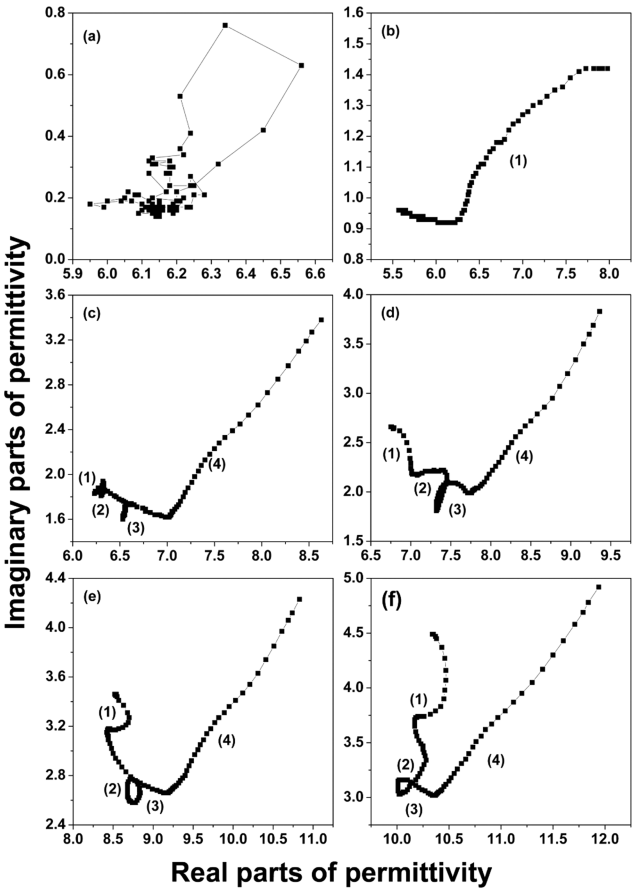

Figure 10. Typical Cole–Cole semicircles (ε'' vs ε') for Fe_3O_4 microspheres (a) and different core–shell Fe_3O_4@C composites (b, S1; c, S2; d, S3; e, S4; f, S5) in the frequency range of 1–18 GHz.

ε'–ε'' curves of Fe_3O_4 microspheres and Fe_3O_4@C core–shell composites in the frequency range of 1–18 GHz. It can be clearly seen that Fe_3O_4 microspheres present a totally disordered curve, implying that there is no obvious dielectric relaxation process. Sample S1 consisted of Fe_3O_4 microspheres and incomplete carbon shell displays only one dielectric relaxation process. Once carbon shells are formed completely, it is very interesting to find out that there are four distinguishable semicircles for S2, S3, S4, and S5, suggesting that the core–shell structure endows these composites with multiple dielectric relaxation processes. On the basis of the results mentioned above, it is believable that the enhancement in microwave absorption of S2, S3, S4, and S5 comes from the increased complex permittivity and improved characteristic

dx.doi.org/10.1021/am502910d | ACS Appl. Mater. Interfaces 2014, 6, 12997−13006

impedance, as well as sufficient interfacial relaxation between Fe_3O_4 microspheres and carbon shell.

According to eq 3, the thickness (d) of an absorber is one of the crucial parameters that affect the intensity and responding frequency of reflection loss; thus, we further investigate the reflection losses of S2−S5 with the different thicknesses of 1.5, 2.0, 2.5, 3.0, 4.0, and 5.0 mm in order to eliminate the influence from the thickness of the samples. As shown in Figure 11, all

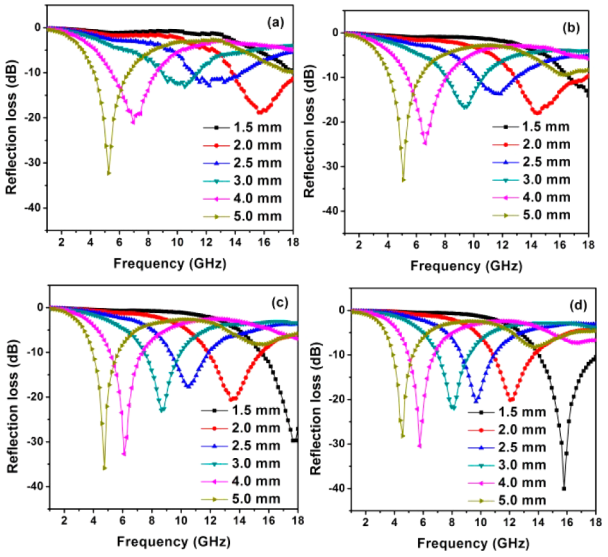

Figure 11. Microwave reflection losses of core−shell Fe_3O_4@C composites S2 (a), S3 (b), S4 (c), and S5 (d) at different absorber thicknesses.

four samples exhibit negative shifts to low frequency with increasing thickness, and their values of reflection loss exceeding −10 dB (90% absorption) can be obtained in the range of 4.0−18 GHz with a variation in thickness from 1.5 to 5.0 mm, indicating excellent microwave absorption properties of these composites. However, S4 and S5 still show superior microwave absorption as compared to S2 and S3, especially in the high frequency range, which may be caused by the improved dielectric loss abilities of S4 and S5 in high frequency range (Figure 6). The strong reflection losses over such wide frequency ranges in S4 and S5 are better than those of some ever reported composites of Fe_3O_4 and various carbon materials.[26−30] A careful look at the reflection loss curves of S4 and S5 reveals that S5 shows much stronger reflection loss than S4 at a thickness of 1.5 mm, and a little stronger at 2.5 mm. However, at other thicknesses, the values of reflection loss for S5 are slightly inferior to those of S4. Considering that some scattered carbon microspheres (Supporting Information Figure S4) and relatively wide distribution of carbon shells thickness (Supporting Information Figure S3) in sample S5 will destroy its chemical homogeneity, thus sample S4 may be taken as the best candidate as a promising microwave absorber in this series.

4. CONCLUSIONS

With Fe_3O_4 microspheres as the cores and nucleation sites, core−shell Fe_3O_4@C composites have been prepared through in situ polymerization of phenolic resin followed by high-temperature carbonization. The thickness of carbon shell can be well controlled by modulating the weight ratios of resorcinol and Fe_3O_4 microspheres. Under the current conditions, the chemical reaction between carbon shell and Fe_3O_4 microspheres is not discovered, but Fe_3O_4 microspheres can promote the graphitization degree of carbon shell. As a result, the crystalline phase and magnetic property of Fe_3O_4 microspheres are well preserved in the final products. Fe_3O_4@C composites show substantially enhanced microwave absorption properties, due to the introduction of dielectric loss, interfacial loss, and improved matching impedance after carbon coating. Besides, core−shell structure endows these composites with an unusual dielectric behavior, leading to strong reflection loss in the high frequency range. We believe this work will be helpful in the design and preparation of highly effective microwave absorbers with improved chemical homogeneity.

■ ASSOCIATED CONTENT

Supporting Information

XRD pattern of the sample carbonized at 700 °C; TEM images of Fe_3O_4 microspheres; low-magnification TEM images and statistical data of Fe_3O_4@C composites; Raman spectrum of phenolic resin carbonized at 650 °C in the absence of Fe_3O_4 microspheres; C_0 values of Fe_3O_4 microspheres and Fe_3O_4@C composites. This material is available free of charge via theInternet at http://pubs.acs.org.

■ AUTHOR INFORMATION

Corresponding Authors

*E-mail:yunchendu@hit.edu.cn.
*E-mail: pxu@hit.edu.cn.

Notes

The authors declare no competing financial interest.

■ ACKNOWLEDGMENTS

This work is supported by National Natural Science Foundation of China (21003029, 21371039, 21101041), China Postdoctoral Science Foundation (2013M541394 and 2014T70341), the Fundamental Research Funds for the Central Universities and Program for Innovation Research of Science in HIT (B201411, HIT.BRETIII.201223), and Natural Science Foundation of Heilongjiang Province (B201405).

■ REFERENCES

(1) Stankovich, S.; Dikin, D. A.; Dommett, G. H. B.; Kohlhaas, K. M.; Zimney, E. J.; Stach, E. A.; Piner, R. D.; Nguyen, S. T.; Ruoff, R. S. Graphene-Based Composite Materials. *Nature* **2006**, *442*, 282−286.

(2) Huang, X.; Qi, X. Y.; Boey, F.; Zhang, H. Graphene-Based Composites. *Chem. Soc. Rev.* **2012**, *41*, 666−686.

(3) Xu, Y. H.; Zhu, Y. J.; Liu, Y. H.; Wang, C. S. Electrochemical Performance of Porous Carbon/Tin Composite Anodes for Sodium-Ion and Lithium-Ion Batteries. *Adv. Energy Mater.* **2013**, *3*, 128−133.

(4) He, Q. L.; Yuan, T. T.; Wei, S. Y.; Haldolaarachchige, N.; Luo, Z. P.; Young, D. P.; Khasanov, A.; Guo, Z. H. Morphology- and Phase-Controlled Iron Oxide Nanoparticles Stabilized with Maleic Anhydride Grafted Polypropylene. *Angew. Chem., Int. Ed.* **2012**, *51*, 8842−8845.

(5) Wang, H. W.; Xu, Z. J.; Yi, H.; Wei, H. G.; Guo, Z. H.; Wang, X. F. One-Step Preparationofsingle-crystalline Fe_2O_3 Particles/Graphene Composite Hydrogels as High Performance Anode Materials for Supercapacitors. *Nano Energy* **2014**, *7*, 86−96.

(6) Zhu, J. H.; Chen, M. J.; Qu, H. L.; Wei, H. G.; Guo, J.; Luo, Z. P.; Haldolaarachchige, N.; Young, D. P.; Wei, S. Y.; Guo, Z. H. Positive and Negative Magnetoresistance Phenomena Observed in Magnetic ElectrospunPolyacrylonitrile-Based Carbon NanocompositeFibers. *J. Mater. Chem. C* **2014**, *2*, 715−722.

(7) He, Q. L.; Yuan, T. T.; Yan, X. R.; Luo, Z. P.; Haldolaarachchige, N.; Young, D. P.; Wei, S. Y.; Guo, Z. H. One-Pot Synthesis of Size-

and Morphology- Controlled 1-D Iron Oxide Nanochains with Manipulated Magnetic Properties. *Chem. Commun.* **2014**, *50*, 201−203.
(8) Zhou, G. M.; Wang, D. W.; Li, F.; Zhang, L. L.; Li, N.; Wu, Z. S.; Wen, L.; Lu, G. Q.; Cheng, H. M. Graphene-Wrapped Fe_3O_4 Anode Material with Improved Reversible Capacity and Cyclic Stability for Lithium Ion Batteries. *Chem. Mater.* **2010**, *22*, 5306−5313.
(9) Liu, J.; Qiao, S. Z.; Hu, Q. H.; Lu, G. Q. Magnetic Nanocomposites with Mesoporous Structures: Synthesis and Applications. *Small* **2011**, *7*, 425−443.
(10) Zou, G. F.; Xiong, K.; Jiang, C. L.; Li, H.; Li, T. W.; Du, J.; Qian, Y. T. Fe_3O_4Nanocrystals with Novel Fractal. *J. Phys. Chem. B* **2005**, *109*, 18356−18360.
(11) Cui, C. K.; Du, Y. C.; Li, T. H.; Zheng, X. Y.; Wang, X. H.; Han, X. J.; Xu, P. Synthesis of Electromagnetic Functionalized Fe_3O_4Microspheres/Polyaniline Composites by Two-Step Oxidative Polymerization. *J. Phys. Chem. B* **2012**, *116*, 9523−9531.
(12) Kaushik, A.; Khan, R.; Solanki, P. R.; Pandey, P.; Alam, J.; Ahmad, S.; Malhotra, B. D. Iron Oxide Nanoparticles-Chitosan Composite Based Glucose Biosensor. *Biosens. Bioelectron.* **2008**, *24*, 676−683.
(13) Shen, S.; Ren, J. F.; Zhu, X. Y.; Pang, Z. Q.; Lu, X. H.; Deng, C. H.; Zhang, R.; Jiang, X. G. MonodisperseMagnetites Anchored onto Carbon Nanotubes: A Platform for Cell Imaging, Magnetic Manipulation and Enhanced Photothermal Treatment of Tumors. *J. Mater. Chem. B* **2013**, *1*, 1939−1946.
(14) Ren, S. H.; Prakash, R.; Wang, D.; Chakravadhanula, V. S. K.; Fichitner, M. Fe_3O_4 Anchored onto Helical Carbon Nanofibers as High-Performance Anode in Lithium-Ion Batteries. *ChemSusChem* **2012**, *5*, 1397−1400.
(15) Kang, E.; Jung, Y. S.; Cavanagh, A. S.; Kim, G. H.; George, S. M.; Dillon, A. C.; Kim, J. K.; Lee, J. W. Fe_3O_4 Nanoparticles Confined in Mesocellular Carbon Foam for High Performance Anode Materials for Lithium-Ion Batteries. *Adv. Funct. Mater.* **2011**, *21*, 2430−2438.
(16) Wang, T. S.; Liu, Z. H.; Lu, M. M.; Wen, B.; Ouyang, Q. Y.; Chen, Y. J.; Zhu, C. L.; Gao, P.; Li, C. Y.; Cao, M. S.; Qi, L. H. Graphene-Fe_3O_4 Nanohybrids: Synthesis and Excellent Electromagnetic Absorption Properties. *J. Appl. Phys.* **2013**, *113*, No. 024314.
(17) Wu, Z. S.; Yang, S. B.; Sun, Y.; Parvez, K.; Feng, X. L.; Mullen, K. 3D Nitrogen-Doped Graphene Aerogel-Supported Fe_3O_4 Nanoparticles as Efficient Eletrocatalysts for the Oxygen Reduction Reaction. *J. Am. Soc. Chem.* **2012**, *134*, 9082−9085.
(18) Wang, G. Z.; Gao, Z.; Tang, S. W.; Chen, C. Q.; Duan, F. F.; Zhao, S. C.; Lin, S. W.; Feng, Y. H.; Zhou, L.; Qin, Y. Microwave Absorption Properties of Carbon Nanocoils Coated with Highly Controlled Magnetic Materials by Atomic Layer Deposition. *ACS Nano* **2010**, *6*, 11009−11017.
(19) Wu, Y.; Wei, Y.; Wang, J. P.; Jiang, K. L.; Fan, S. S. Conformal Fe_3O_4 Sheath on Aligned Carbon Nanotube Scaffolds as High-Performance Anodes for Lithium Ion Batteries. *Nano Lett.* **2013**, *13*, 818−823.
(20) Xuan, S. H.; Hao, L. Y.; Jiang, W. Q.; Gong, X. L.; Hu, Y.; Chen, Z. Y. A Facile Method to Fabricate Carbon-Encapsulated Fe_3O_4 Core/Shell Composites. *Nanotechnology* **2007**, *18*, No. 035602.
(21) Li, L.; Wang, T. T.; Zhang, L. Y.; Su, Z. M.; Wang, C. G.; Wang, R. S. Selected-Control Synthesis of Monodisperse Fe_3O_4@C Core-Shell Spheres, Chains, and Rings as High-Performance Anode Materials for Lithium-Ion Batteries. *Chem.—Eur. J.* **2012**, *18*, 11417−11422.
(22) An, Q.; Zhang, P.; Li, J. M.; Ma, W. F.; Guo, J.; Hu, J.; Wang, C. C. Silver-Coated Magnetite-Carbon Core-Shell Microspheres as Substrate-Enhanced SERS Probes for Detection of Trace Persistent Organic Pollutants. *Nanoscale* **2012**, *4*, 5210−5216.
(23) Zhang, X. B.; Tong, H. W.; Liu, S. M.; Yong, G. P.; Guan, Y. F. An Improved Stober Method towards Uniform and Monodisperse Fe_3O_4@C Nanospheres. *J. Mater. Chem. A* **2013**, *1*, 7488−7493.
(24) You, L. J.; Xu, S.; Ma, W. F.; Li, D.; Zhang, Y. T.; Guo, J.; Hu, J. J.; Wang, C. C. Ultrafast Hydrothermal Synthesis of High Quality Magnetic Core Phenol-Formaldehyde Shell Composite Microspheres Using the Microwave Method. *Langmuir* **2012**, *28*, 10565−10572.
(25) Kong, L. R.; Lu, X. F.; Bian, X. J.; Zhang, W. J.; Wang, C. Constructing Carbon-Coated Fe_3O_4 Microspheres as Antiacid and Magnetic Support for Palladium Nanoparticles for Catalytic Applications. *ACS Appl. Mater. Interfaces* **2011**, *3*, 35−42.
(26) Jin, Y. H.; Seo, S. D.; Shim, H. W.; Park, K. S.; Kim, D. W. Synthesis of Core/Shell Spinel Ferrite/Carbon Nanoparticles with Enhanced Cycling Stability for Lithium Ion Battery Anodes. *Nanotechnology* **2012**, *23*, 125204.
(27) Wang, L. L.; Liang, J. W.; Zhu, Y. C.; Mei, T.; Zhang, X.; Yang, Q.; Qian, Y. T. Synthesis of Fe_3O_4@C Core-Shell Nanorings and Their Enhanced Electrochemical Performance for Lithium-Ion Batteries. *Nanoscale* **2013**, *5*, 3627−3631.
(28) Zheng, F. C.; Chen, Q. W.; Hu, L.; Yan, N.; Kong, X. K. Synthesis of Sulfonic Acid-Functionalized Fe_3O_4@C Nanoparticles as Magnetically Recyclable Solid Acid Catalysts for Acetalization reaction. *Dalton Trans.* **2014**, *43*, 1220−1227.
(29) Huang, X.; Lu, M.; Zhang, X.; Wen, G.; Zhou, Y.; Fei, L. Carbon Microtube/Fe_3O_4Nanocomposite with Improved Wave-Absorbing Performance. *Scr. Mater.* **2012**, *67*, 613−616.
(30) Ni, S. B.; Wang, X. H.; Guo, Z.; Feng, Y.; Wang, J. M.; He, D. Y. Designed Synthesis of Wide Range Microwave Absorption Fe_3O_4-Carbon Sphere Composite. *J. Alloys Compd.* **2010**, *489*, 252−256.
(31) Li, X. H.; Yi, H. B.; Zhang, J. W.; Feng, J.; Li, F. S.; Xue, D. S.; Zhang, H. L.; Peng, Y.; Mellors, N. J. Fe_3O_4-Graphene Hybrids: Nanoscale Characterization and Their Enhanced Electromagnetic Wave Absorption in Gigahertz Range. *J. Nanopart. Res.* **2013**, *15*, 1472.
(32) Zheng, J.; Lv, H. L.; Lin, X. H.; Ji, G. B.; Li, X. G.; Du, Y. W. Enhanced Microwave Electromagnetic Properties of Fe_3O_4/GrapheneNanosheet Composites. *J. Alloys Compd.* **2014**, *589*, 174−181.
(33) Hekmatara, H.; Seifi, M.; Forooraghi, K. Microwave Absorption Property of Aligned MWCNT/Fe_3O_4. *J. Magn. Magn. Mater.* **2013**, *346*, 186−191.
(34) Chen, Y. J.; Xiao, G.; Wang, T. S.; Ouyang, Q. Y.; Qi, L. H.; Ma, Y.; Gao, P.; Zhu, C. L.; Cao, M. S.; Jin, H. B. Porous Fe_3O_4/Carbon Core/Shell Nanorods: Synthesis and Electromagnetic Properties. *J. Phys. Chem. C* **2011**, *115*, 13603−13608.
(35) Zhang, B.; Du, Y. C.; Zhang, P.; Zhao, H. T.; Kang, L. L.; Han, X. J.; Xu, P. Microwave Absorption Enhancement of Fe_3O_4/Polyaniline Core/Shell Hybrid Microspheres with Controlled Shell Thickness. *J. Appl. Polym. Sci.* **2013**, *130*, 1909−1916.
(36) Meng, Y.; Gu, D.; Zhang, F. Q.; Shi, Y. F.; Yang, H. F.; Li, Z.; Yu, C. Z.; Tu, B.; Zhao, D. Y. Ordered Mesoporous Polymers and Homologous Carbon Frameworks: Amphiphilic Surfactant Templating and Direct Transformation. *Angew. Chem., Int. Ed.* **2005**, *44*, 7053−7059.
(37) Sun, Z. H.; Wang, L. F.; Liu, P. P.; Wang, S. C.; Sun, B.; Jiang, D. Z.; Xiao, F. S. Magnetically Motive Porous Sphere Composite and Its Excellent Properties for the Removal of Pollutants in Water by Adsorption and Desorption Cycles. *Adv. Mater.* **2006**, *18*, 1968−1971.
(38) Zhao, H. T.; Du, Y. C.; Kang, L. L.; Xu, P.; Du, L.; Sun, Z. H.; Han, X. J. Precursor-Directed Synthesis of Quasi-Spherical Barium Ferrite Particles with Good Dispersion and Magnetic Properties. *CrystEngComm* **2013**, *15*, 808−815.
(39) Yang, Z. H.; Li, Z. W.; Zhao, J.; Yang, Y. H. Synthesis and Enhanced Microwave Properties of Uniform Hollow Fe Nanospheres and Their Core-Shell Silica Nanocomposites. *RSC Adv.* **2014**, *4*, 9457−9462.
(40) Chen, D.; Xu, R. Hydrothermal Synthesis and Characterization of Nanocrystalline Fe_3O_4 Powders. *Mater. Res. Bull.* **1998**, *33*, 1015−1021.
(41) Deng, Y. H.; Deng, C. H.; Qi, D. W.; Liu, C.; Liu, J.; Zhang, X. M.; Zhao, D. Y. Synthesis of Core/Shell Colloidal Magnetic Zeolite Microspheres for the Immobilization of Trypsin. *Adv. Mater.* **2009**, *21*, 1377−1382.
(42) Song, Q.; Zhang, Z. J. Correlation between Spin-Orbital Coupling and the Superparamagnetic Properties in Magnetite and

Cobalt Ferrite Spinel Nanocrystals. *J. Phys. Chem. B* **2006**, *110*, 11205−11209.
(43) Du, Y. C.; Wang, J. Y.; Cui, C. K.; Liu, X. R.; Wang, X. H.; Han, X. J. Pure Carbon Microwave Absorbers from Anion-Exchange Resin Pyrolysis. *Synth. Met.* **2010**, *160*, 2191−2196.
(44) Du, Y. C.; Liu, T.; Yu, B.; Gao, H. B.; Xu, P.; Wang, J. Y.; Wang, X. H.; Han, X. J. The Electromagnetic Properties and Microwave Absorption of Mesoporous Carbon. *Mater. Chem. Phys.* **2012**, *135*, 884−891.
(45) Nemanich, R. J.; Solin, S. A. First- and Second-Order Raman Scattering from Finite-Size Crystals of Graphite. *Phys. Rev. B* **1979**, *20*, 392−401.
(46) Dillon, R. O.; Woollam, J. A.; Katkanant, V. Use of Raman Scattering to Investigate Disorder and Crystallite Formation in As-Deposited and Annealed Carbon Films. *Phys. Rev. B* **1984**, *29*, 3482−3489.
(47) Ferrari, A. C.; Robertson, J. Interpretation of Raman Spectra of Disordered and Amorphous Carbon. *Phys. Rev. B* **2000**, *61*, 14095−14107.
(48) Wang, K. X.; Wang, Y. G.; Wang, Y. R.; Hosono, E.; Zhou, H. S. Mesoporous Carbon Nanofibers for Supercapacitor Application. *J. Phys. Chem. C* **2009**, *113*, 1093−1097.
(49) Chen, N.; Mu, G. H.; Pan, X. F.; Gan, K. K.; Gu, M. Y. Microwave Absorption Properties of $SrFe_{12}O_{19}/ZnFe_2O_4$ Composite Powders. *Mater. Sci. Eng., B* **2007**, *139*, 256−260.
(50) Zhang, P.; Han, X. J.; Kang, L. L.; Qiang, R.; Liu, W. W.; Du, Y. C. Synthesis and Characterization of Polyaniline Nanoparticles with Enhanced Microwave Absorption. *RSC Adv.* **2013**, *3*, 12694−12701.
(51) Xu, P.; Han, X. J.; Wang, C.; Zhou, D. H.; Lv, Z. S.; Wen, A. H.; Wang, X. H.; Zhang, B. Synthesis of Electromagnetic Functionalized Nickel/Polypyrrole Core/Shell Composites. *J. Phys. Chem. B* **2008**, *112*, 10443−10448.
(52) Wang, C.; Han, X. J.; Xu, P.; Zhang, X. L.; Du, Y. C.; Hu, S. R.; Wang, J. Y.; Wang, X. H. The Electromagnetic Property of Chemically Reduced Graphene Oxide and Its Application as Microwave Absorbing Material. *Appl. Phys. Lett.* **2011**, *98*, No. 072906.
(53) Tang, N. J.; Zhong, W.; Au, C. T.; Yang, Y.; Han, M. G.; Lin, K. L.; Du, Y. W. Synthesis, Microwave Electromagnetic, and Microwave Absorption Properties of Twin Carbon Nanocoils. *J. Phys. Chem. C* **2008**, *112*, 19316−19323.
(54) Wang, Z. J.; Wu, L. N.; Zhou, J. G.; Shen, B. Z.; Jiang, Z. H. Magnetite Nanocrystals on Multiwalled Carbon Nanotubes as a Synergistic Microwave Absorber. *J. Phys. Chem. C* **2013**, *117*, 5446−5452.
(55) Cao, M. S.; Song, W. L.; Hou, Z. L.; Wen, B.; Yuan, J. The Effects of Temperature and Frequency on the Dielectric Properties, Electromagnetic Interference Shielding and Microwave-Absorption of Short Carbon Fiber/Silica Composites. *Carbon* **2010**, *48*, 788−796.
(56) Zhao, X. C.; Zhang, Z. M.; Wang, L. Y.; Xi, K.; Cao, Q. Q.; Wang, D. H.; Yang, Y.; Du, Y. W. Excellent Microwave Absorption Property of Graphene-Coated Fe Nanocomposites. *Sci. Rep.* **2013**, *3*, 3421.
(57) Jiang, J. J.; Li, D.; Geng, D. Y.; An, J.; He, J.; Liu, W.; Zhang, Z. D. Microwave Absorption Properties of Core Double-Shell FeCo/C/$BaTiO_3$Nanocomposites. *Nanoscale* **2014**, *6*, 3967−3971.
(58) Sunny, V.; Kumar, D. S.; Mohanan, P.; Anantharaman, M. R. Nickel/Carbon Hybrid Nanostructures as Microwave Absorbers. *Mater. Lett.* **2010**, *64*, 1130−1132.
(59) Zou, T. C.; Li, H. P.; Zhao, N. Q.; Shi, C. S. Electromagnetic and Microwave Absorbing Properties of Multi-Walled Carbon Nanotubes Filled with Ni Nanowire. *J. Alloys Compd.* **2010**, *496*, L22−L24.
(60) Pisani, L.; Montanari, B.; Harrison, N. M. A Defective Graphene Phase Predicted to Be A Room Temperature Ferromagnetic Semiconductor. *New J. Phys.* **2008**, *10*, No. 033002.
(61) Zhou, W. C.; Hu, X. J.; Sun, C. H.; Yan, J.; Zhou, S. Y.; Chen, P. Microwave Absorbing Properties of Fe_3O_4-Poly(3, 4-ethylenedioxythiophene) Hybrids in Low-Frequency Band. *Polym. Adv. Technol.* **2014**, *25*, 83−88.
(62) Lu, B.; Dong, X. L.; Huang, H.; Zhang, X. F.; Zhu, X. G.; Lei, J. P.; Sun, J. P. Microwave Absorption Properties of the Core/Shell-Type Iron and Nickel Nanoparticles. *J. Magn. Magn. Mater.* **2008**, *320*, 1106−1111.
(63) Wu, M. Z.; Zhang, Y. D.; Hui, S.; Xiao, T. D.; Ge, S. H.; Hines, W. A.; Budnick, J. I.; Taylor, G. W. Microwave Magnetic Properties of $Co_{50}/(SiO_2)_{50}$ Nanoparticles. *Appl. Phys. Lett.* **2002**, *80*, 4404−4406.
(64) Zhu, J. H.; Wei, S. Y.; Haldolaarachchige, N.; Young, D. P.; Guo, Z. H. Electromagnetic Field Shielding Polyurethane Nanocomposites Reinforced with Core-Shell Fe-Silica Nanoparticles. *J. Phys. Chem. C* **2011**, *115*, 15304−15310.
(65) Zhu, C. L.; Zhang, M. L.; Qiao, Y. J.; Xiao, G.; Zhang, F.; Chen, Y. J. Fe_3O_4/TiO_2 Core/Shell Nanotubes: Synthesis and Magnetic and Electromagnetic Wave Absorption Characteristics. *J. Phys. Chem. C* **2010**, *114*, 16229−16235.
(66) Xu, P.; Han, X. J.; Liu, X. R.; Zhang, B.; Wang, C.; Wang, X. H. A Study of the Magnetic and Electromagnetic Properties of Gamma-Fe_2O_3-Multiwalled Carbon Nanotubes (MWCNT) and Fe/Fe_3C-MWCNT Composites. *Mater. Chem. Phys.* **2009**, *114*, 556−560.